Combined bearing faults detection using the Multiple Improved Envelope Spectra via Feature Optimization gram (MIESFO-gram) in complex systems

Mahsa Yazdanianasr, Alexandre Mauricio, Konstantinos Gryllias

Combined bearing faults detection using the Multiple Improved Envelope Spectra via Feature Optimization gram (MIESFO-gram) in complex systems

Mahsa YAZDANIANASR[1,2], Alexandre MAURICIO[1,2], Konstantinos GRYLLIAS [1,2]

[1]Department of Mechanical Engineering, KU Leuven,
Celestijnenlaan 300, Box 2420, 3001 Leuven, Belgium
[2]Flanders Make@KU Leuven, 3001 Leuven, Belgium
mahsa.yazdanianasr@kuleuven.be

Abstract

Bearing diagnostics is a growing field of study, with a focus on complex machinery that includes a variety of bearing and gear components operating under varying conditions (e.g. speed and load). Meanwhile, some components with weak signatures may remain hidden while others with intensive defects are detected. Therefore, the ability to detect combined faults in the machinery, having different cyclic frequencies is critical. Envelope Analysis is a popular method for bearing diagnostics, in which a filter is typically applied around an excited frequency band and the signal is enveloped, yielding the Squared Envelope Spectrum. However, as several damaged bearings may excite not only different but also several frequency bands simultaneously, band-pass filtering around only one frequency band may not be sufficient to detect all bearing faults in the machine. This will be more challenging when an operational condition like speed is changing over time which causes the fault-related cyclic frequencies to be smeared and/or hidden. Furthermore, different carrier frequencies may be excited under different speed conditions. Recently, IESFOgram has been proposed utilizing Targeted and Blind features. The method has been essentially developed based on either the Cyclic Spectral Correlation or the Cyclic Spectral Coherence, in order to select the optimal frequency band and extract the corresponding Improved Envelope Spectrum. In the IESFOgram with the Targeted features, the possible existing fault frequencies are fed into the algorithm as inputs. However, the IESFOgram with Blind features aims to find the most-occupied frequency band with the cyclic frequencies. On the other hand, when there are more than one bearing faults exciting different natural frequencies, selecting only the single most dominant carrier may prove insufficient to detect other damages present in the signals. In this paper, an extension of the Blind IESFOgram is introduced with the aim of finding all possible unique frequency bands occupied by cyclic frequencies. The method is applied and evaluated on simulated and experimental data with different types of faults under steady and varying speed conditions in a complex system. Finally, the results are compared with the conventional Targeted and Blind IESFOgram.

1 Introduction

Rolling element bearings play a pivotal role in the functioning of rotating equipment. Failure to timely detect any potential damage in bearings can significantly hinder the accurate planning of maintenance interventions. In the worst-case scenario, this can result in catastrophic failures, substantial production losses, and an escalation in overall costs. Therefore, it is crucial to promptly identify any impairment to ensure effective maintenance planning and mitigate the risks. Hence, vibration-based condition monitoring serves as a highly effective approach for diagnosing bearing faults, complementing maintenance strategies aiming at identifying potential machine malfunctions. Nevertheless, signal processing within this context encounters formidable challenges when applied to complex machinery, where multiple concurrent factors contribute to the characterization of the machine's condition. A significant consideration lies in the fact that the signatures emitting from bearing fault signatures are typically obscured amidst a diverse range of noise sources and more dominant components such as gears. Moreover, within the domain of complex machinery, the presence of multiple rolling

bearings operating in close proximity is common. Consequently, it is imperative to meticulously explore and identify all potential faults, as some may possess weaker signatures yet still pose a significant risk comparable to faults with more prominent signatures. Examples of these intricate machinery systems are abundant in industrial domains, including wind turbine drive trains, power generation facilities, mining sectors, agricultural enterprises, etc. Hence, there is a need to employ a robust signal processing methodology for effective fault diagnosis within complex systems.

In the realm of bearing diagnostics, the traditional practice of utilizing envelope analysis has long been employed. The fundamental principle of envelope analysis involves the demodulation of signals by subjecting them to a band-pass filter, which restricts the frequency range to a specific interval. Nevertheless, an ongoing question among analysts pertains to the optimal range for applying a band-pass filter to effectively observe the bearing fault signatures. Typically, the vibration signals are filtered around their resonance frequencies, which are stimulated by damaged impulses. These resonance frequencies essentially act as carrier frequencies for the modulation frequencies. The aim is to achieve an optimal filter band that exhibits a high Signal-to-Noise ratio (SNR), resulting in a filtered Squared Envelope Spectrum (SES). This spectral representation effectively amplifies the fault harmonics [1, 2]. Recently, researchers have been striving to develop (semi-) automated approaches for the selection of an optimal frequency band, thereby surpassing the reliance on purely subjective engineering knowledge in the context of filtering applications. One of the well-known methods of automated band selection tools is the Fast Kurtogram [3] where the band selection is done based on the maximum kurtosis level. Also, an enhanced version of the Fast Kurtogram (FK), known as the Protugram, has been introduced [4]. The Protugram improves upon the FK methodology by extracting the maximum kurtosis from the envelope signal rather than the raw signal. The Sparsogram approach [5] operates on evaluating the sparsity levels across various frequency bands using wavelet-packet analysis. On the other hand, the Infogram technique [6] utilizes Negentropy as a feature to identify the impulsive frequency bands within the signal, facilitating the subsequent demodulation. Additionally, the Autogram [7], relies on the concept of maximum kurtosis. However, the Autogram distinguishes itself from the Fast Kurtogram (FK) by computing the maximum kurtosis using the unbiased autocorrelation of the squared envelope derived. It utilized the (undecimated) Maximal Overlap Discrete Wavelet Packet Transform (MODWPT) to split the signal into frequency bands. Also, they concluded that multi-band integration is needed by combining filtered Squared Envelope Spectra (SES) with the highest kurtosis at each level, resulting in the Combined Squared Envelope Spectrum (CSES).

Conversely, over the past two decades, the Cyclic Spectral Correlation (CSC) and the Cyclic Spectral Coherence (CSCoh) have emerged as alternatives to SES-based methods [8, 9, 10]. A noteworthy advantage of the CSC and CSCoh methods lies in their capability to reveal hidden periodicity associated with second-order cyclostationarity, such as bearing signals that may be obscured by stronger signals and noise. These methods represent the signals in bi-variable maps within the frequency-frequency domain, enabling integration along the spectral axis to obtain either the Enhanced Envelope Spectrum (EES) or the Improved Envelope Spectrum (IES). The bi-variable maps generated by CSC and CSCoh require expert scrutiny to manually select the optimal band for spectral axis integration, leading to the generation of the Improved Envelope Spectrum (IES). To address this limitation, a recent solution known as the IESFOgram using Targeted and Blind Features [11, 12] has been proposed as an automated band selection tool for the bi-variable maps produced by the CSC and the CSCoh. The efficacy of this method was evaluated under challenging circumstances like low-speed conditions or in the presence of non-Gaussian noise [13, 14] which may exist in complex systems. Furthermore, the IESFOgram Targeted approach has been expanded by incorporating a weighting strategy to emphasize bands with higher Targeted feature within the 1/3 binary tree levels, enabling the construction of the Combined Improved Envelope Spectrum (CIES) in [15]. However, a notable limitation remains when prior knowledge about cyclostationary signals of different intensities but equal importance is unavailable. Therefore, for such blind investigation of combined faults, a first objective is not to merge the informative bands but rather to individually explore the potential bands to capture any hidden information they may contain. This paper aims to address the challenge of identifying separate frequency bands associated with diverse fault-induced signatures, without prior knowledge. Specifically, the aim is to discern faults with weaker signatures, which tend to be obscured in comparison to stronger faults during combined fault scenarios. The rest of the paper is outlined as follows. In Section 2, the background theory of cyclostationarity is described. In Section 3, the proposed methodology is presented. In Section 4, the methodology is evaluated using both simulated and experimental data. The paper closes in Section 5 with some conclusions.

2 Theory of cyclostationarity

Rotating mechanical components have a tendency to generate cyclical transient signatures that exhibit periodicity when the rotational speed remains constant during signal acquisition. These signals often contain valuable information regarding the condition of machine elements, making signal processing and feature extraction crucial for defect detection and monitoring. In line with the principles of cyclostationary theory, the signals acquired from rotating machinery can be effectively characterized by the presence of the first two orders of cyclostationarity Signals characterized by first-order cyclostationarity (CS_1) exhibit a periodic behavior in their first-order statistical moment as a function of time (T) that conforms to the conditions specified by Eq. 1:

$$C_{1x}(t) = \mathbb{E}\{x(t)\} = C_{1x}(t+T) \tag{1}$$

In the given equation, the operator $\mathbb{E}$ represents the ensemble averaging, while t represents time and T represents the period. In the context of rotating machinery, vibrations signals characterized by first-order cyclostationarity (CS_1) exhibit periodic waveforms that are associated with specific components and are phase-locked to the rotor speed. Examples of such phenomena include shaft misalignment and spalling on meshing gears. On the other hand, a second-order cyclostationary (CS_2) signal is defined as a signal whose second-order statistical moment is periodic, specifically demonstrated by the periodicity of its autocorrelation function with a period of T, as described in Eq. 2:

$$C_{2x}(\tau,t) = \mathbb{E}\{x(t)x(t-\tau)^*\} = C_{2x}(\tau,t+T) \tag{2}$$

In the context provided, the variable t represents the continuously sampled time, while τ represents the time delay. The symbol $\mathbb{E}$ corresponds to the expected value or the ensemble average. Bearing vibration signals are commonly classified as second-order cyclostationary (CS_2) signals, owing to their underlying periodicity associated with the rotational speed of the shaft. Signals exhibiting higher orders of cyclostationarity, such as CS_n where n is greater than 2, are not typically considered in the analysis of rotating machinery. This is because CS_1 and CS_2 adequately capture the essential characteristics of the signals generated by such machinery.

The Cyclic Spectral Correlation (CSC) is an analytical technique that effectively characterizes signals exhibiting first-order (CS_1) and second-order (CS_2) cyclostationarity in the frequency-frequency domain. This method is formulated as a distribution function involving two frequency variables: the cyclic frequency α, which is associated with modulation, and the spectral frequency f, which is linked to the carrier signal.

The tool can be described also as the correlation distribution of the carrier and modulation frequencies of the signatures present in the signals, defined in Eq. 3:

$$CSC(\alpha,f) = \lim_{W\to+\infty} \frac{1}{W}\mathbb{E}\{F_w[x(t)]F_w[x(t+\tau)]^*\} \tag{3}$$

where $F_w[x(t)]$ indicates the spectrum of the signal $x(t)$ over a finite time duration of W using the Fourier Transform. By normalizing the Cyclic Spectral Correlation, the definition of the Cyclic Spectral Coherence $(CSCoh)$ is derived as in Eq. 4:

$$CSCoh(\alpha,f) = \frac{CSC(\alpha,f)}{\sqrt{CSC(0,f)CSC(0,f+\alpha)}} \tag{4}$$

Both the Cyclic Spectral Correlation (CSC) and the Cyclic Spectral Coherence (CSCoh) bi-variable maps can be integrated over the spectral frequency axis to derive a spectrum. This integration process yields a one-dimensional spectrum function called Improved Envelope Spectrum (IES) which is solely dependent on the cyclic frequency α as shown in Eq. 5:

$$IES(\alpha) = \frac{1}{F_2-F_1}\int_{F_1}^{F_2} |CSCoh(\alpha,f)|df \tag{5}$$

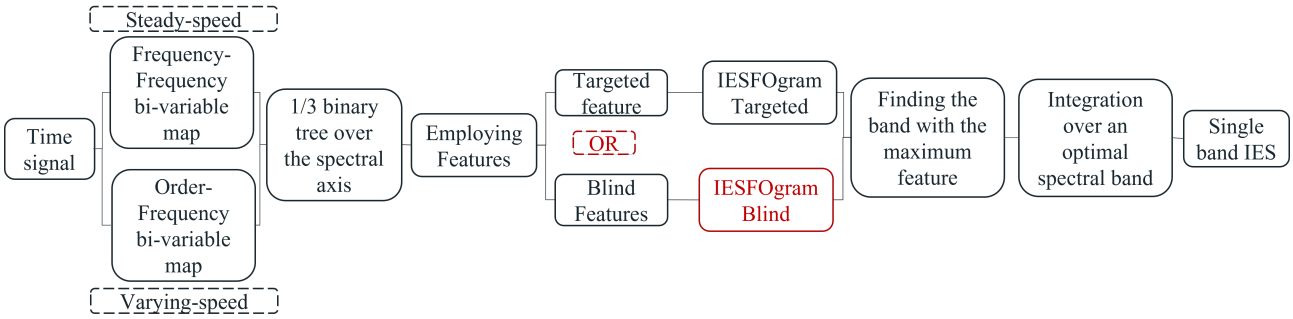

Figure 1: Schematic diagram of the IESFOgram algorithm

The Improved Envelope Spectrum via Feature Optimization-gram (IESFOgram)[11]is a recently proposed band selection tool which can be applied on the bi-variable map, as presented in the scheme depicted in Figure 1. The IESFOgram Targeted feature tries to optimize a Normalized Diagnostic Feature (NDF) based on the cyclic characteristics of interest (e.g. rolling element bearing characteristic fault frequencies/orders) on the spectrum resulting from the integration of the bi-variable map. Moreover, the Blind IESFOgram employs some statistical features on the bi-variable map to choose the optimum band. The method is thought to be general enough to be applied to either the CSC or the CSCoh.

3 Proposed methodology

The utilization of bi-variable maps for diagnostic purposes necessitates a thorough understanding of the map to effectively extract and exploit its embedded information. In contrast, one-dimensional spectra analysis is more prevalent in both academic and industrial settings, owing to its simplicity and widespread application. However, integrating the bi-variable function along its spectral variable yields a one-dimensional spectrum, which can serve as a valuable diagnostic tool in its own right. Nevertheless, it is crucial to acknowledge that diagnostic insights within the integrated spectrum can potentially be obscured by the presence of noise and the overlapping signatures of other components. Therefore, careful analysis and interpretation are required to disentangle and uncover the desired diagnostic information from these potential sources of interference. The process of integrating the specific frequency band that contains the desired signal can significantly improve the spectral characteristics and enhance the detection capability for the target frequencies. This approach can effectively boost the performance and the sensitivity in identifying the frequencies of interest. In practical implementations, multiple faults associated with distinct carrier frequencies and varying levels of insensitivity may manifest. Moreover, fluctuating operating conditions, such as varying speed and load, can influence the identification of carrier frequencies across different frequency bands. Consequently, it becomes imperative to adopt a multifaceted approach encompassing multiple frequency bands in order to comprehensively investigate potential characteristic frequencies rather than limiting the analysis to a single optimal band. To tackle this issue, the current research paper introduces a novel approach known as Multiple Improved Envelope Spectra via Feature Optimization-gram (MIESFOgram). The subsequent sections will outline a detailed, step-by-step explanation of the method's process.

Stage 1: In the initial stage, the bi-variable map is derived from the signal using various estimators, such as the Averaged Cyclic Periodogram (ACP), the Cyclic Modulation Spectrum (CMS), the Fast Spectral Correlation (FSC), or alternative numerical techniques, as referenced in [12]. This process facilitates the extraction of the CSC bi-variable map, as described in Equation 3. The normalized version of CSC, denoted as CSCoh, can serve as a substitution for the original CSC representation. Notably, these bi-variable maps manifest in the frequency-frequency domains. Furthermore, in the presence of varying speed conditions, these estimators adhere to a similar principle; however, there are some variations. Specifically, the modulation signals will be expressed in the order domain using angular re-sampling methods, while the bi-variable maps will be represented in the order-frequency domains. These adjustments account for the dynamic nature of speed variations and enhance the applicability of the estimators in such scenarios. The users have the option to select their preferred approach for acquiring the bi-variable map based on methods in [16, 17]. These references are indicated as numerical

implementations of the CSC in the Order-Frequency domain. Also in the reference [9] Fast Spectral Correlation (FSC) was suggested as a provider of the CSC in the Frequency-Frequency domain with good performance. Additionally, when the method is employed on the order-tracked signal with respect to angle, it yields the Order-Order domain.

Stage 2: The subsequent stage involves segmenting the map based on the spectral axis f using a 1/3-binary tree structure, which is analogous to the one employed in the Fast Kurtogram [3]. The division of the map is accomplished through the utilization of individual trees characterized by decreasing bandwidth (Bw) and incrementally varying center frequencies (Cf). These parameters, in turn, establish the upper and lower limits (f_1 and f_2) required for the integration process described in Equation 5. Subsequently, the integration of each band within the map yields a demodulated equivalent spectrum known as the Improved Envelope Spectrum (IES).

Stage 3: During this stage, where there is a lack of prior knowledge regarding the characteristic frequencies of faults, Blind features are employed. This approach draws inspiration from the conventional Blind IESFOgram as depicted in Figure 1. The utilized features encompass statistical parameters, including Kurtosis, Spectral Negentropy, Spectral Flatness, L2/L1 Norm, and Gini index. For a comprehensive understanding of the mathematical formulation of these Blind features, further details can be found in the references provided in [13].

This is the stage in the conventional Blind IESFOgram where the optimal band is chosen by maximizing the Blind feature. However, when multiple fault signatures simultaneously are present across different carrier frequencies throughout the spectral band, relying solely on the selection of a single optimal band becomes insufficient. In such cases, the algorithm will fail to capture the frequency bands that exhibit weak fault signatures across various frequency ranges. Subsequent stages will be undertaken to address and resolve this concern.

Stage 4: The objective of this step is to study the frequency bands (which will be called nodes in this paper) in the 1/3 binary tree that takes values based on the Blind Feature $BF(Cf_N, Bw_N)$ in the vector with the length equal to the number of nodes N and Cf_N and Bw_N being the center frequency and the bandwidth of the node N respectively. Therefore, in this stage, the nodes will be sorted ($SBF(Cf_N, Bw_N)$) based on the Blind feature from the maximum to the minimum. Afterward, all Improved Envelope Spectra (IESs) for all nodes based on the SBF are stored in the IES_{SBF}.

Stage 5: The core of the solution is applied in this stage where the correlation matrix is extracted from the IES_{SBF} for N nodes. The correlation matrix can have the size of $(N \times N)$ in the largest size. However, a smaller correlation matrix with size $(M \times M)$ from the initial nodes can represent dominant nodes in the spectral bands. Therefore, each value a_{M1} in the correlation matrix will be calculated as follows:

$$a_{M1} = \frac{\sum_{i=1}^{\alpha}(x_i - \bar{x})(y_i - \bar{y})}{\sqrt{\sum_{i=1}^{\alpha}(x_i - \bar{x})^2}\sqrt{\sum_{i=1}^{\alpha}(y_i - \bar{y})^2}} \tag{6}$$

where $x = IES_{SBF}(M, \alpha)$ and $y = IES_{SBF}(1, \alpha)$ respectively. In this way, the correlation matrix of the Multiple Improved Envelope Spectra via Feature Optimization gram (MIESFOgram) will be constructed as follows:

$$\mathbf{A} = \begin{bmatrix} a_{11} & a_{12} & \cdots & a_{1M} \\ a_{21} & a_{22} & \cdots & a_{2M} \\ \vdots & \vdots & \ddots & \vdots \\ a_{M1} & a_{M2} & \cdots & a_{MM} \end{bmatrix} \tag{7}$$

where $\mathbf{A} \in \mathbb{R}^{M \times M}$ and $M < N$. In the correlation matrix of the MIESFOgram, the diagonal elements always have a value of 1, indicating the correlation of an individual IES signal with itself. The off-diagonal elements represent the similarity between different pairs of IES signals. As a result, it is expected that certain rows and columns in the correlation matrix may exhibit low correlation values with most of the IES spectra, except for the intersections with their corresponding pairs in which they demonstrate high similarity. These specific intersection points within the matrix can provide insights into weaker cyclic signatures that may be less prominent compared to stronger components.

Stage 6: To rank the rows with high to low correlation values, the summation of correlation values in each

row of the matrix **A** is calculated and then sorted in a descending way as Equation(8):

$$\text{sorted\_rows} = \text{sort}\left(\sum_{i=1}^{M} \mathbf{A}[i,:],' descend'\right) \tag{8}$$

where $\mathbf{A}[i,:]$ represents the ith row in MIESFOgram's Correlation Matrix. Consequently, the sorted_rows will exhibit a noticeable decrease, indicating the presence of weaker signatures that are ranked lower. These values are clearly distinguishable when there exists a significant disparity between the strong and weak signature components, as observed in combined faults where distinct characteristic frequencies manifest in the IES. The dominance of one intensive frequency tends to obscure the other components within the signature. Ultimately, by computing the average of the sorted rows, two distinct groups can be delineated. Alternatively, one can apply clustering methods to effectively partition the data in an appropriate manner.

Stage 7: During the concluding phase, within each cluster, the node possessing the highest Blind feature among the $BF_{(1\times N)}(Cf_N, Bw_N)$ vector is identified and reported. This yields multiple IES spectra that reveal distinct components in the bi-variable map without prior knowledge. By comparing the identified peaks within these multiple IES spectra to the potential characteristic frequencies within the machine, one can establish correspondences between the signatures and components in the complex system.

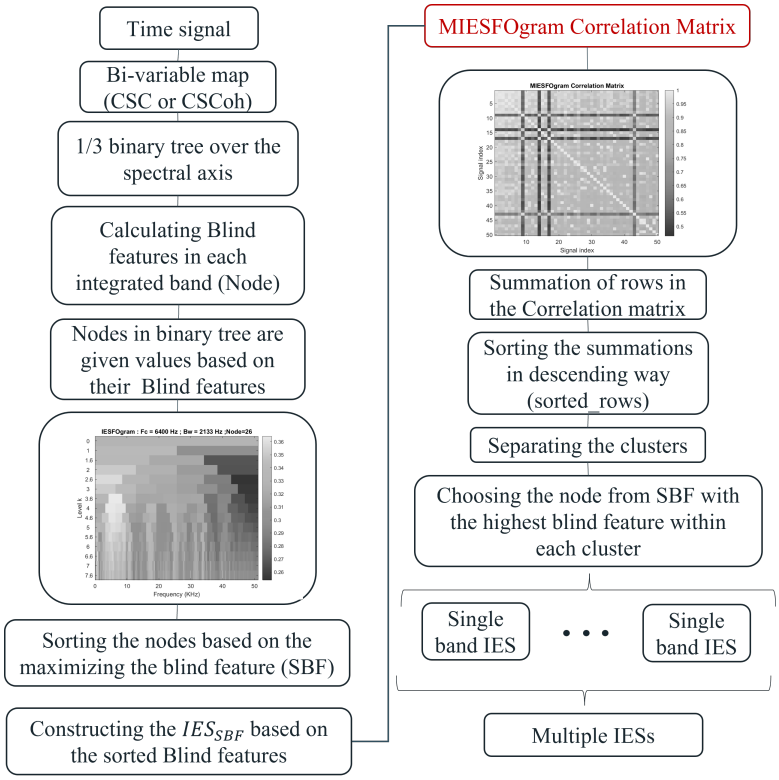

Figure 2: Schematic diagram of the MIESFOgram algorithm

4 Experimental applications and results

4.1 Simulated signal of combined faults

Within this section, the proposed methodology will be initially evaluated through the application of a simulated signal. The signal generated utilizing the phenomenological model [18], encompasses two distinct fault types, including an inner race and an outer race defect. The first component of the signal is simulated to replicate the occurrence of an inner race fault (BPFI) based on the geometric properties of a deep groove ball bearing identified as SKF 6208. Similarly, the second component is generated to imitate an outer race fault (BPFO) using the specifications of a double-row self-aligning bearing known as SKF 2206 ETN9. The detail information of the bearing's geometries has been listed in Table 1.

	B_D (mm)	P_D (mm)	# of Balls	BPFI factor	BPFO factor
SKF 2206	10	47.022	12	7.276	4.724
SKF 6208	12.3	60	9	5.423	3.577

Table 1: Geometry specification of the bearing and their characteristic frequency factors

In the simulation of the signal, several factors are taken into account. Firstly, the signal was generated at a speed of 8.42 Hz. Moreover, white Gaussian noise was intentionally introduced, simulating the presence of background interference. The amplitudes of the signal are carefully adjusted to ensure that the Enhanced Envelope Spectrum (EES), which represents the integration over the entire frequency band, exhibits peaks of BPFO harmonics but BPFI signatures are below the noise threshold level. It is important to highlight that all figures in this paper include the depiction of the noise threshold, which is calculated based on three times the Moving Absolute Deviation (MAD) of each spectrum [19]. In addition, diverse carrier frequencies are assigned to introduce multiple excited carrier frequencies within the signal. The comprehensive information regarding the modulation and the corresponding carrier frequencies together with the signal specifications can be found in Table 2.

	Shaft speed (Hz)	Signal length (Sec)	Modulation frequency (Hz)	Carrier Frequency (KHz)	Sampling Frequency(KHz)
Outer race fault SKF 2206	8.42	10	39.77	40	102.4
Inner race fault SKF 6208	8.42	10	45.66	1	102.4

Table 2: Specifications of the simulated signal containing both BPFI and BPFO signatures

For the signal analysis process, the IESFOgram Targeted methods are applied to examine both the Ball Pass Frequency of the Inner race (BPFI) and the Ball Pass Frequency of the Outer race (BPFO). As illustrated in Figure 3, a modulation by the BPFO at a frequency of 39.77Hz is identified at the frequency band with central frequency equal to 38.4 kHz and bandwidth 12.8 kHz. Additionally, Figure 4 reveals the identification of a double modulation by the frequency of 45.66 Hz, which corresponds to the BPFI, and by the shaft rotating speed of 8.42 Hz.

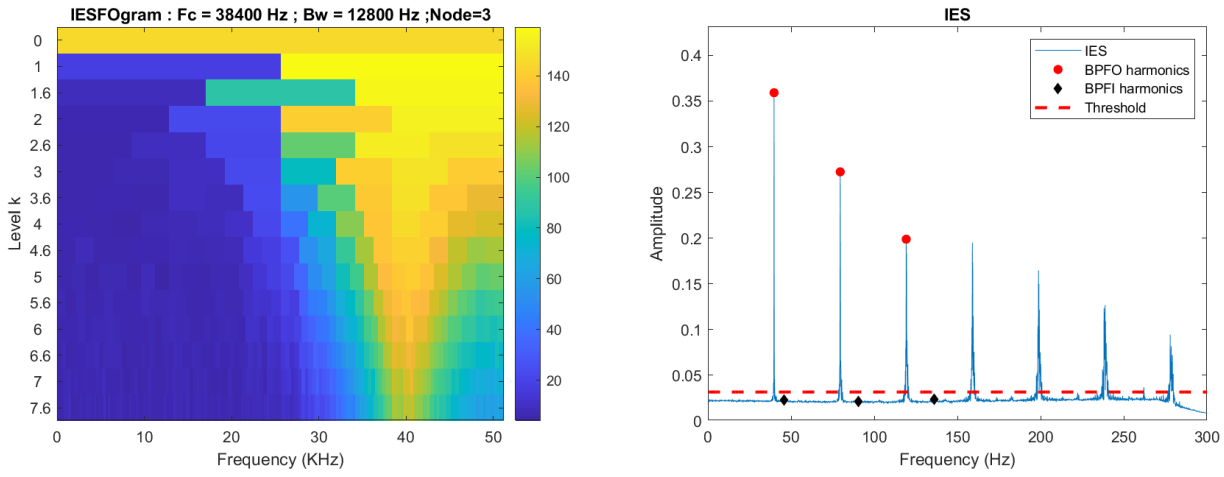

(a) Targeted IESFOgram to BPFO

(b) Targeted IES to BPFO

Figure 3: Targeted IESFOgram and IES to BPFO for a simulated signal

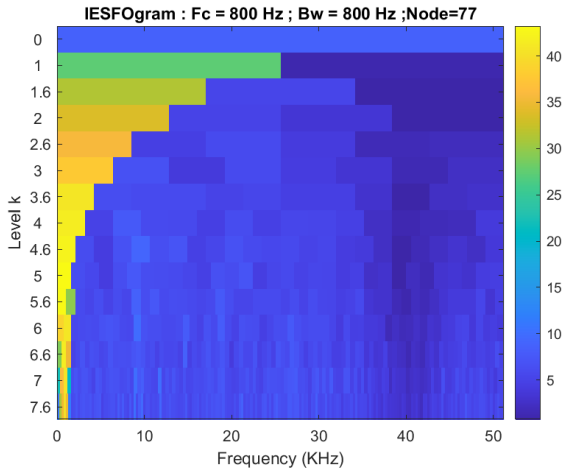

(a) Targeted IESFOgram to BPFI

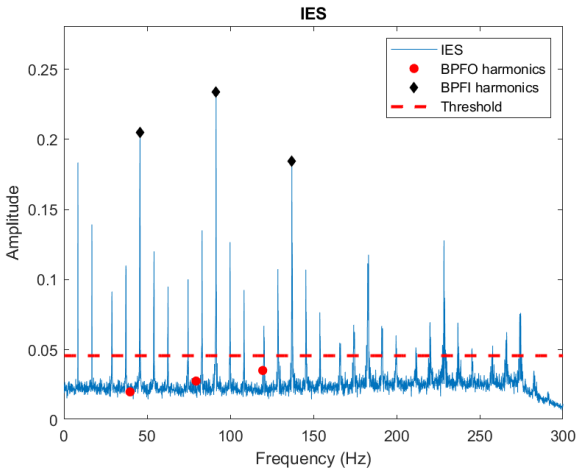

(b) Targeted IES to BPFI

Figure 4: Targeted IESFOgram and IES to BPFI for a simulated signal

Subsequently, the Blind IESFOgram, employing the Gini index, is applied to the signal without any prior knowledge. The Gini index, renowned for its robust performance in the IESFOgram, serves as a statistical feature. For detailed information on the calculation of this feature, the reader is referred to the work cited in [13]. The results are shown in Figure 5. As it is illustrated in the Figure 5a, the assignment of values to the nodes has been meticulously carried out, taking into consideration the presence of the predefined carrier frequencies. However, due to the dominant presence of the BPFO signature in the simulated signal and the conventional approach employed by the Blind IESFOgram, which selects only one optimal band, the alternative band encompassing the faint signature of BPFI remains concealed and unchosen. Consequently, the peaks that are expected to correspond to the BPFI remain undetectable. It is important to emphasize that, at this stage, the conventional Blind IESFOgram chooses the optimal band by selecting the node with the highest Gini index and then blindly extracts the IES of that band without any prior indication of fault frequencies. However, in order to comprehensively assess the method's performance, the peaks at the characteristic frequencies and their harmonics are shown in the IES in Figure 5b.

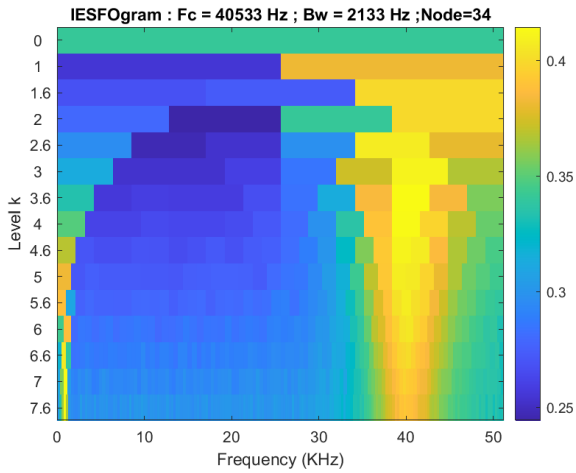

(a) Blind IESFOgram using Gini index

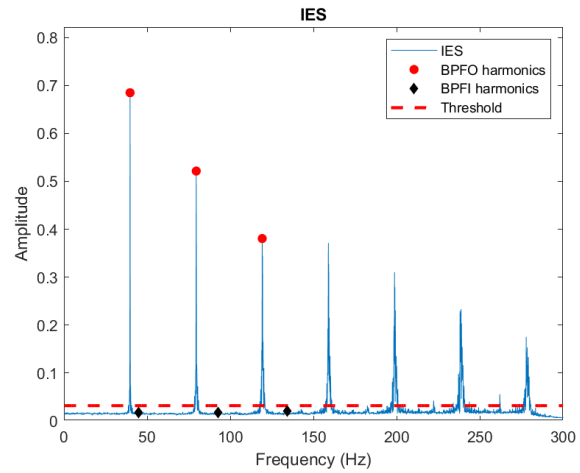

(b) Blind IES using the Gini index

Figure 5: Blind IESFOgram and IES using Gini index for simulated signal

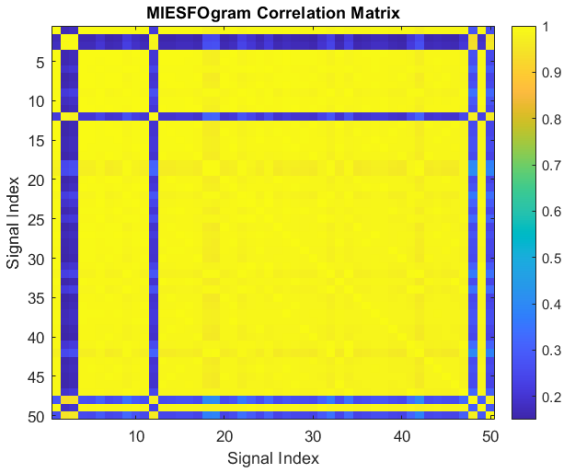

(a) MIESFOgram Correlation Matrix

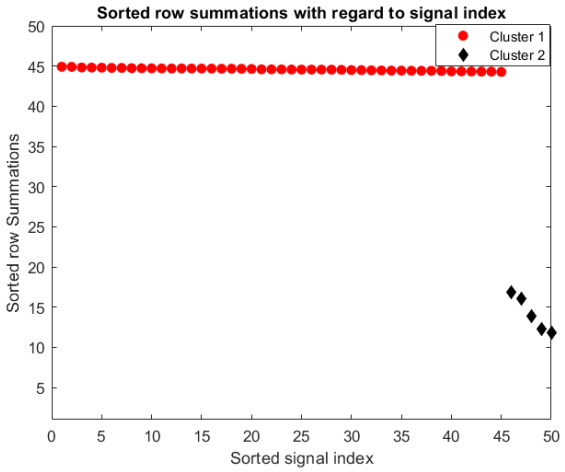

(b) Sorted row summations in function of the signal index

Figure 6: MIESFOgram Correlation Matrix and the sorted row summations in function to the signal index for simulated signal

To address this issue, a solution has been proposed as described in Section 3, wherein the nodes are organized based on maximizing the Blind Gini index values. Subsequently, the IESs were extracted for each node and the corresponding Sorted Blind features SBF and the IES_{SBF} were calculated. To construct the MIESFOgram Correlation matrix, the user can select a group of initial IESs, as stated in Stage 5 of the methodology. Figure 6a showcases the resultant MIESFOgram Correlation Matrix for the first 50 nodes. An analysis of the figure reveals that a significant portion of the IESs exhibits strong correlations with one another, indicating their classification within a shared cluster of behavior in the bi-variable map. However, it is evident from the MIESFOgram Correlation Matrix that there exist some IESs that display weak correlations with a significant portion of other IESs, as indicated by the darker-colored lines. Interestingly, these lines intersect at specific regions where the correlation values are notably high, suggesting a notable similarity among the corresponding IESs.

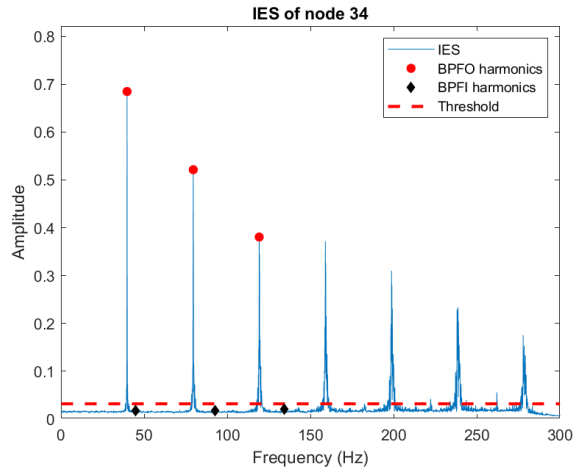

(a) IES of the node from cluster 1 with the highest Gini index

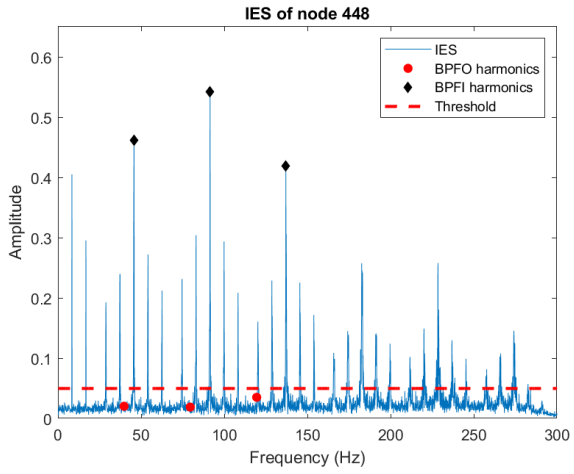

(b) IES of the node from cluster 2 with the highest Gini index

Figure 7: IES of the nodes with the highest Gini index in each cluster

Consequently, in accordance with the explanation provided in Stage 6 of the methodology, the summations

of each row in the MIESFOgram Correlation Matrix were computed and arranged in descending order. The graphical representation in Figure 6b demonstrates that cluster 1 primarily consists of nodes exhibiting a high correlation, while cluster 2 encompasses nodes with lower correlation values. Importantly, these two clusters are distinctly separated based on the total mean value. In conclusion, as elucidated in Stage 7 of the methodology, the node exhibiting the highest blind Gini index within each cluster was selected based on *SBF* as the representative of the prevailing components present in the signals. The outcomes of this selection process are presented in Figure 7. Consequently, the identification of the second weaker component of the BPFI occurs in node 448, in contrast to the previously discovered node 34 which exemplifies the BPFO in the simulated signal.

4.2 Application of the methodology on a complex system with combined faults

This section presents the evaluation of the methodology using real experimental data acquired from the KU Leuven Diagnostic Test rig, as depicted in Figure 8. The test rig comprised an electric drive motor, a first housing containing a healthy bearing, a disk for the installation of an unbalanced weight, a second housing with large damage to the outer race of the test bearing, a double row self-aligned bearing SKF 2206 ETN9, and two gearboxes. Notably, the input shaft of the first gearbox incorporates a deep groove ball bearing SKF 6208 exhibiting inner race fault damage. The detailed information of the bearings has been mentioned in Table 1. The test rig was tested at $f_{shaft} = 8.42\ Hz$. Two ICP accelerometers (PCB-model number 352A10), were mounted on the housing of the bearing and on the gearbox casing in close proximity to the faulty bearing.

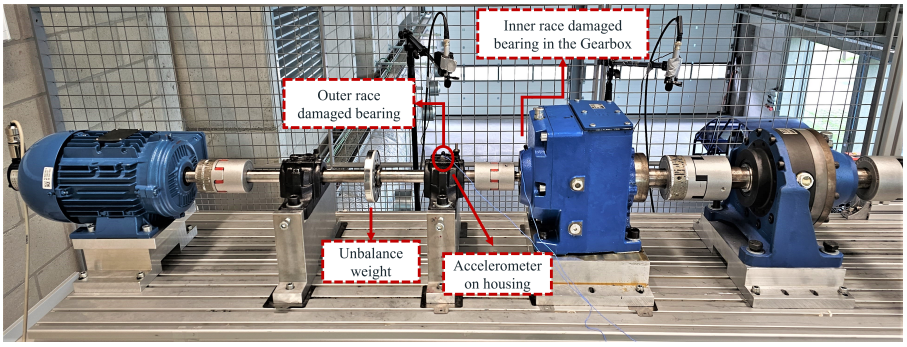

Figure 8: KU Leuven Diagnostic test rig

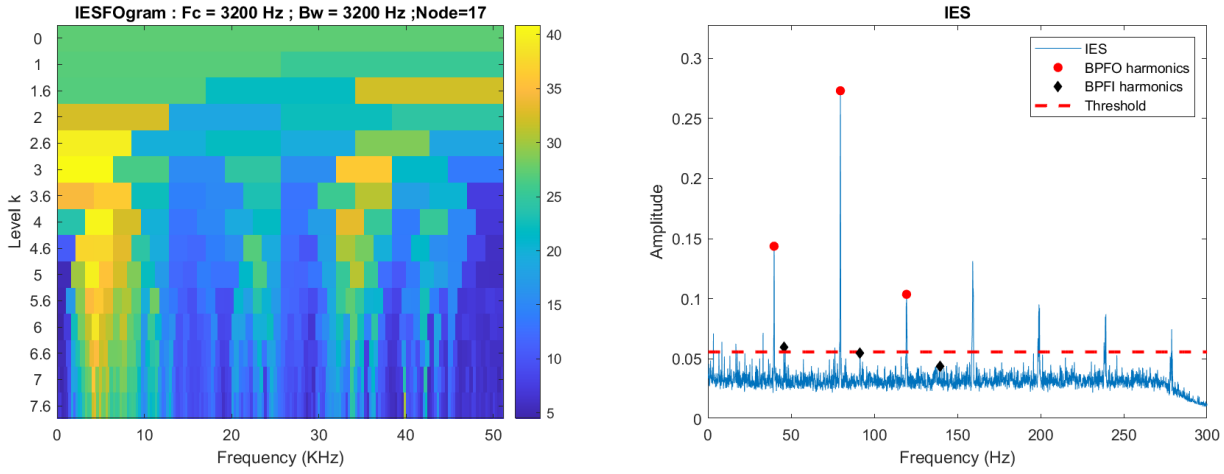

(a) Targeted IESFOgram to BPFO

(b) Targeted IES to BPFO

Figure 9: Targeted IESFOgram and IES to BPFO on an experimental signal

The objective of the experiment is to identify both faults mentioned earlier by utilizing the signal obtained from the accelerometer positioned on the top part of the bearing housing exhibiting large damage to the outer

race. By examining the signal using the Targeted IESFOgram and inputting the frequencies associated with the BPFI and the BPFO, the presence of the BPFO can be identified, as illustrated in Figure 9. Moreover, the BPFI of the bearing within the gearbox can also be determined, as demonstrated in Figure 10.

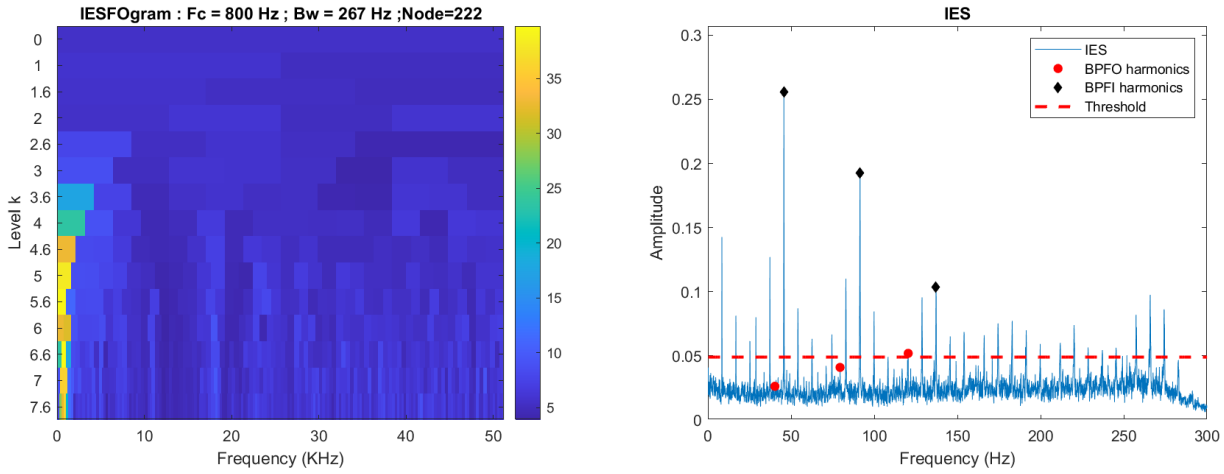

(a) Targeted IESFOgram to BPFI

(b) Targeted IES to BPFI

Figure 10: Targeted IESFOmap and IES to BPFI on an experimental signal

Nonetheless, when utilizing the Blind IESFOgram with the Gini index, only a single optimal frequency band was selected, resulting in a clear depiction of the BPFO signature in the spectrum, as shown in Figure 11. However, this approach may not be adequate for scenarios involving combined fault cases. It is important to note that in the blind method, the frequencies of the faults are not known in advance. However, for the purpose of demonstrating the method's performance, the figures include data points corresponding to both faults and their harmonics.

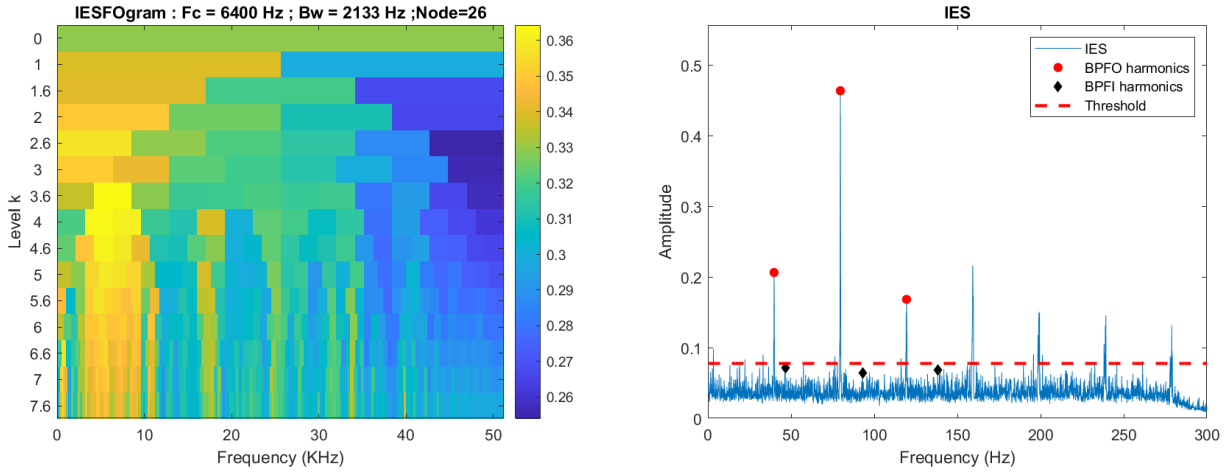

(a) Blind IESFOgram using the Gini index

(b) Blind IES using the Gini index

Figure 11: Blind IESFOgram and IES using the Gini index on an experimental signal

To tackle this problem, the MIESFOgram method was applied and the correlation matrix was extracted as shown in Figure 12a. Then, the summation of values in each of the rows was calculated and sorted. The result is shown in Figure 12b which illustrates two separate clusters.

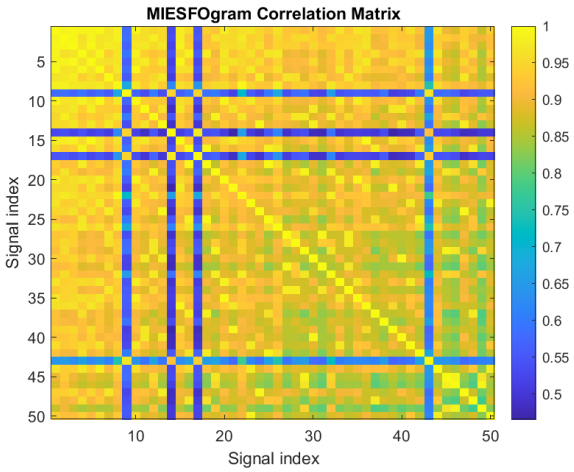

(a) MIESFOgram Correlation Matrix

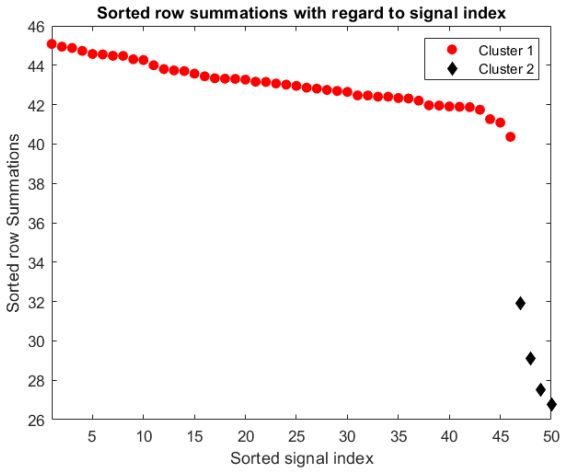

(b) Sorted row summations in function to the signal index

Figure 12: MIESFOgram Correlation Matrix and the sorted row summations for an experimental signal

In conclusion, the nodes characterized by the highest Gini index within each cluster were identified and presented as the multiple Improved Envelope Spectra (Multiple IES), as are depicted in Figure 13.

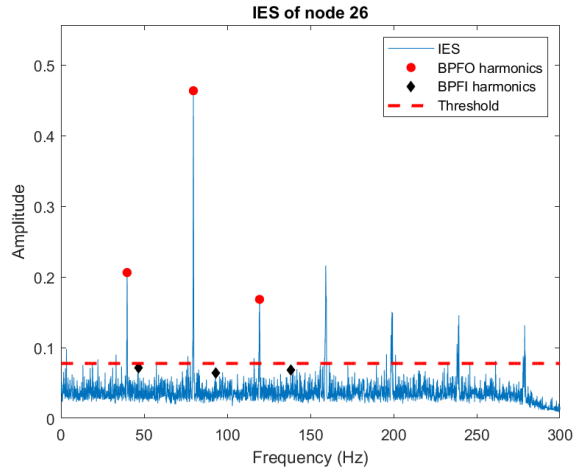

(a) IES of the node from cluster 1 with the highest Gini index

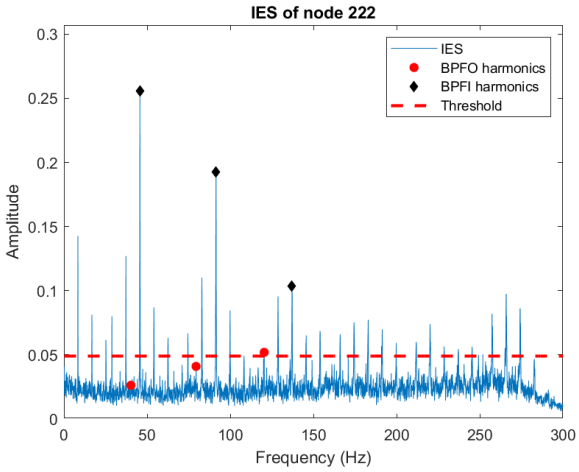

(b) IES of the node from cluster 2 with the highest Gini index

Figure 13: IES of the nodes with the highest Gini index in each cluster

As previously stated, the MIESFOgram algorithm is versatile and can be applied to bi-variable maps derived from various estimators, regardless of whether they belong to the frequency-frequency domain in steady speed conditions or the order-frequency domain in varying speed scenarios. Consequently, the method was also employed on a signal captured under a randomly varying speed profile. The raw time signal and the random varying speed profile are depicted in Figure 14.

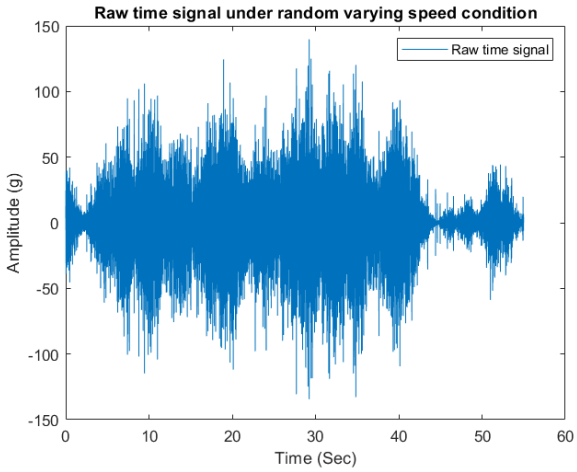

(a) Raw time signal

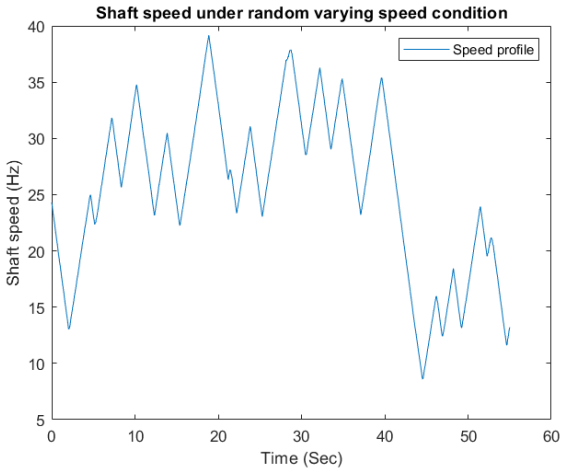

(b) Random varying speed profile

Figure 14: Raw time signal and the speed profile of experimental data captured at random varying speed condition

Considering that the signal was acquired under varying speed conditions, an angular resampling procedure was performed. Subsequently, an Order Frequency Cyclic Modulation Spectrum (OFCMS) bi-variable map was extracted. The application of the IESFOgram Blind feature Gini index, as illustrated in Figure 15, successfully identifies the optimal band that contains the BPFO component, similar to the steady speed case. Consequently, the subsequent steps involve the application of the MIESFOgram method, resulting in the extraction of the correlation matrix, as demonstrated in Figure 16.

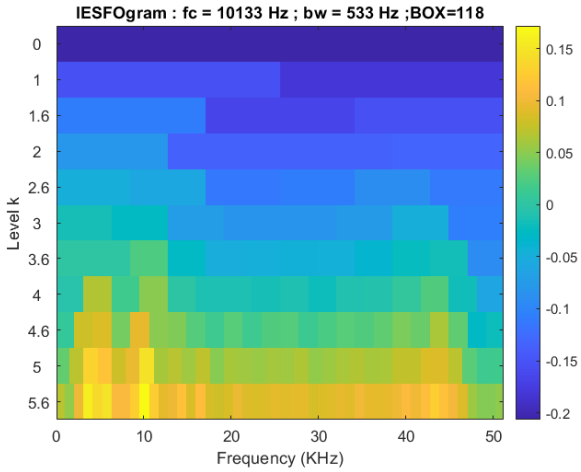

(a) Blind IESFOgram using the Gini index

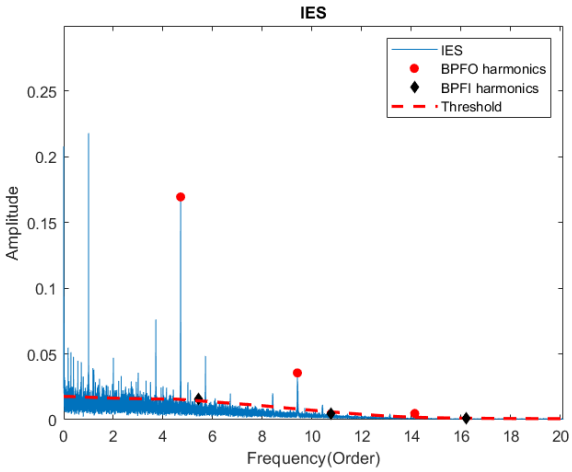

(b) Blind IES using the Gini index

Figure 15: IESFOgram extracted from the OFCMS and Blind IES using the Gini index at a signal captured under varying speed

The presence of darker lines exhibiting high correlation intersections suggests the existence of additional cyclostationary clusters. By performing row summation and subsequent value sorting on the correlation matrix, nodes with the highest Gini index pertaining to each cluster were identified and reported. The outcomes, depicting multiple Improved Envelope Spectra (IESs), are presented in Figure 17. As a result of this analysis, the node containing the signatures of the BPFI was also detected, as illustrated in Figure 17b.

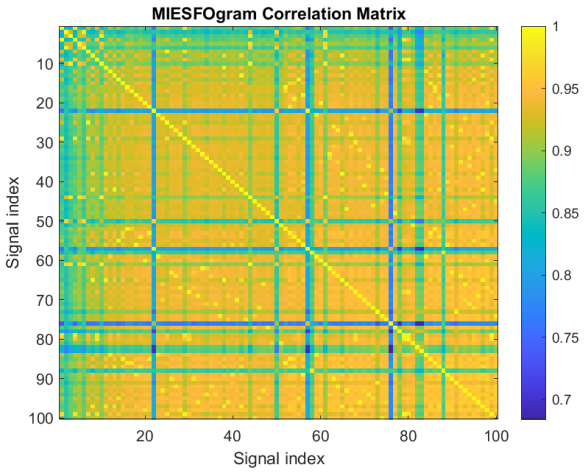

(a) MIESFOgram Correlation Matrix

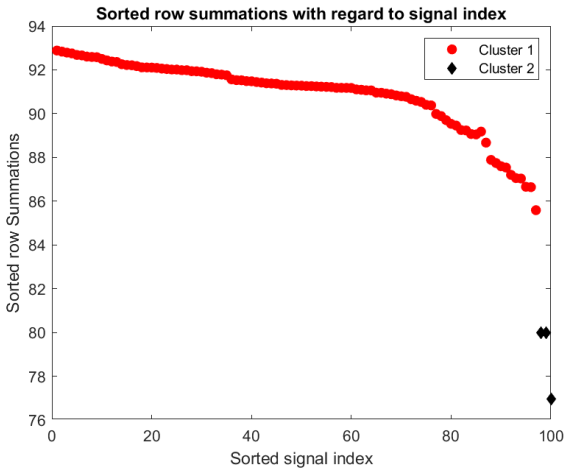

(b) Sorted row summations in function to the signal index

Figure 16: MIESFOgram Correlation Matrix and the sorted row summations under varying speed condition

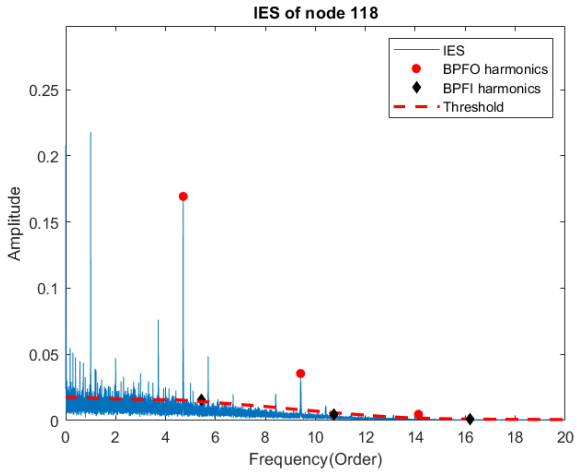

(a) IES of the node from cluster 1 with the highest Gini index

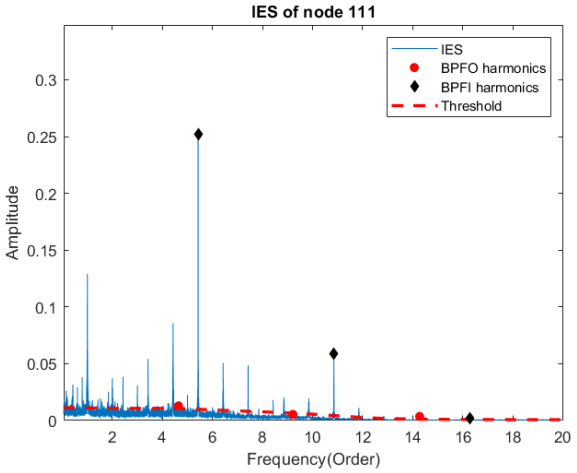

(b) IES of the node from cluster 2 with the highest Gini index

Figure 17: IES of the nodes with the highest Gini index in each cluster

5 Conclusion

This research paper introduces a novel approach called MIESFOgram for the detection of combined bearing faults. The proposed method aims to identify these faults by presenting multiple Improved Envelope Spectra as the final outcomes. Real-world applications typically involve complex machinery comprising diverse bearing and gear components that operate under varying conditions. In scenarios where multiple faults coexist, certain components with subtle signatures may remain concealed, while others exhibiting severe defects can be detected effectively. The MIESFOgram algorithm is developed by exploiting the inherent cyclo-stationary nature of bearing damages, characterized by a periodic autocorrelation function. Consequently, the correlation distribution of carrier and modulation frequencies in bi-variable maps is utilized as an effective tool for detecting cyclo-stationary signals. By integrating the spectral axis of these bi-variable maps, one can successfully extract the Improved Envelope spectra that capture the modulation frequencies of the carriers within the designated frequency range. In recent studies, approaches have attempted to evaluate various frequency bands

by blindly examining their statistical characteristics, aiming to identify the optimal band within the bi-variable maps. However, when dealing with combined faults, it has been observed that a single band is inadequate for effectively distinguishing all cyclo-stationarities with varying intensities. The MIESFOgram algorithm incorporates a blind approach to construct the correlation matrix, focusing on the highest statistical features within a specific frequency band. This methodology facilitates the examination of distinct clusters of similar Improved Envelope Spectra (IESs) and, as a result, enables the identification of multiple IESs that encompass diverse cyclo-stationary patterns present in the signal. Subsequently, the analyst gains access to multiple frequency bands, thereby enabling the examination of peak values and their harmonics in relation to characteristic frequencies that may exist within the machinery. This facilitates the identification of faulty components. Importantly, this method can be utilized with any type of estimator to extract the bi-variable data which provides sufficient information about the signal. This research paper presents an evaluation of the proposed method using both simulated and experimental data. The simulation was conducted to incorporate inner race and outer race defects, deliberately designing one defect to be indistinguishable from the other. Furthermore, the proposed method was applied to the experimental data obtained from a complex system comprising faulty bearings, gearboxes, and unbalanced components. The evaluation encompassed both the frequency-frequency domain analysis at a constant speed and the order-frequency domain analysis at varying speeds. The results demonstrate that MIESFOgram successfully discerns the presence of a concealed cluster of faults and provides multiple Improved Envelope Spectra (IESs) instead of focusing solely on a single informative frequency band.

Acknowledgements

The authors gratefully acknowledge the Research Foundation Flanders (FWO) under the ROBUSTIFY research grant no. S006119N.

References

[1] R. Randall, J. Antoni, *Rolling element bearing diagnostics: A tutorial*, Mechanical systems and signal processing, Vol. 24, 2011, pp. 485-520.

[2] M. Feldman, *Hilbert transform applications in mechanical vibration*, John Wiley and Sons, 2011.

[3] J. Antoni, *Fast computation of the kurtogram for the detection of transient faults*, Mechanical systems and signal processing, Vol. 21, 2007, pp. 108-124.

[4] T. Barszcz, A. JabLonski, *A novel method for the optimal band selection for vibration signal demodulation and comparison with the Kurtogram*, Mechanical systems and signal processing, Vol. 25, 2011, pp. 431-451.

[5] P.W. Tse, w.Dong, *The sparsogram: A new and effective method for extracting bearing fault features*, Prognostics and System Health Management Conference, 2011, pp. 1-10.

[6] J. Antoni, *The infogram: Entropic evidence of the signature of repetitive transients*, Mechanical systems and signal processing, Vol. 74, 2016, pp. 73-94.

[7] A. Moshrefzadeh, Al. Fasana, *The autogram: an effective approach for selecting optimal demodulation band in rolling element bearings diagnosis*, Mechanical systems and signal processing, Vol. 105, 2017, pp. 294-318.

[8] R. Randall, J. Antoni, S. Chobsaard, *The relationship between spectral correlation and envelope analysis in the diagnostics of bearing faults and other cyclostationary machine signals*, Mechanical systems and signal processing, Vol. 15, 2001, pp. 945-962.

[9] J. Antoni, G. Xin, N. Hamzaoui, *Fast computation of the spectral correlation*, Mechanical systems and signal processing, Vol. 92, 2017, pp. 248-277.

[10] J. Antoni, *Cyclic spectral analysis in practice*, Mechanical systems and signal processing, Vol. 21, 2017, pp. 597-630.

[11] Al. Mauricio, W.A. Smith, J. Qi, R.B. Randall, K. Gryllias, *Cyclo-non-stationarity based bearings diagnostics of planetary bearings*, CMMNO, Santander, Spain, 2018, June 20-22, pp. 1-10.

[12] A. Mauricio, J. Qi, W.A. Smith, M. Sarazin, R.B. Randall, K. Janssens, K. Gryllias, *Bearing diagnostics under strong electromagnetic interference based on Integrated Spectral Coherence*, Mechanical systems and signal processing, Vol. 140, 2020, pp. 2860-2867.

[13] M. Yazdanianasr, Al. Mauricio, K. Gryllias, *Evaluation of the Improved Envelope Spectrum via Feature Optimization-gram (IESFOgram) for bearing diagnostics under low rotating speeds*, Condition Monitor. Machinery Non-Stationary Oper. (CMMNO), 2021 June, pp. 319-324.

[14] M. Yazdanianasr, Al. Mauricio, R. Zimroz, A. Wyłomańska, Agnieszka, K. Gryllias, *Evaluation of the improved envelope spectrum via feature optimization-gram (IESFOgram) for bearing diagnostics in presence of non-Gaussian noise*, Proceedings of ISMA 2022 International Conference on Noise and Vibration Engineering, Leuven, Belgium, 2022.

[15] Al. Mauricio, K. Gryllias *Cyclostationary-based multiband envelope spectra extraction for bearing diagnostics: the combined improved envelope spectrum*, Mechanical systems and signal processing, Vol. 149, 2021, pp. 107-150.

[16] D. Abboud, S. Baudin, J. Antoni, D. Rémond, M. Eltabach, O. Sauvage, *The spectral analysis of cyclo-non-stationary signals*, Mechanical systems and signal processing, Vol. 75, 2016, pp. 280-300.

[17] D. Abboud, J. Antoni, *Order-frequency analysis of machine signals*, Mechanical systems and signal processing, Vol. 87, 2017, pp. 229-258.

[18] G. D Élia, M. Cocconcelli, E. Mucchi, R. Rubini, G. Dalpiaz, *Step-by-step algorithm for the simulation of faulted bear-ings in non-stationary conditions*, ISMA 2016, Leuven, Belgium, pp. 2393-2408.

[19] J. Antoni, F. Bonnardot, A. Raad, M. El Badaoui, *Cyclostationary modelling of rotating machine vibration signals*, Mechanical systems and signal processing, Vol. 18, 2004, pp. 1285-1314.